

Chapter 3

Biom mineralization: Mechanisms of Hydroxyapatite Crystal Growth

Kazuo Onuma, Toru Tsuji, and Mayumi Iijima

Abstract Progress in the investigation of the growth mechanism of hydroxyapatite, the most important biomineral, is described in relation to observation and measurement techniques of crystals growing in aqueous solutions. Optical interferometry, especially phase-shift interferometry, can measure the apatite growth rate precisely and facilitates estimates of several growth parameters necessary to analyze the growth mechanism of apatite. The data strongly suggest that the growth unit of apatite takes the form of energetically stable clusters. Apatite growth proceeds via accumulation of clusters, resembling the growth of macromolecular protein crystals, although conventional spiral or two-dimensional nucleation growth occurs on the surface, as in the case of protein crystals. Phase transformation of amorphous calcium phosphate into apatite proceeds via direct structure reconstruction of aggregates with clusters as the minimum unit. These cluster-based transformation and growth phenomena are not specific to apatite: they also occur in other biominerals, such as calcium carbonates.

Keywords Biom mineralization • Hydroxyapatite • Growth mechanism • Phase-shift interferometry • Cluster

K. Onuma (✉)

National Institute of Advanced Industrial Science & Technology, Central 6,
1-1-1 Higashi, Tsukuba, Ibaraki, 305-8566, Japan
e-mail: k.onuma@aist.go.jp

T. Tsuji

Advanced Research Centers, Keio University, 3-14-1, Hiyoshi, Kohoku-ku,
Yokohama, 223-8522, Japan
e-mail: toruts2002@yahoo.co.jp

M. Iijima

Asahi University School of Dentistry, Oral Functional Science and Rehabilitation,
Dental Materials Science, 1851-1 Hozumi, Mizuho, Gifu, 501-0296, Japan
e-mail: ijijima@dent.asahi-u.ac.jp

3.1 Introduction

The production of crystals or amorphous materials resulting from the interactions of organic and inorganic substances that accompany biological activity within living organisms is known as biomineralization. These living organisms can be both lower and higher organisms, including humans. The production of calcium salt crystals (calcium oxalate) within plants was first described in the 1600s. Therefore, viewed from a historical perspective, biomineralization is an academic field with an extremely long life span.

Narrowly defined, biomineralization is the process by which inorganic substances are produced on organic templates within an organism. Representative examples include the formation of bone and teeth within the human body and the formation of sea urchin spines and shells. Single crystals of apatite, a calcium phosphate, are arranged in human bone possesses an organization in which single crystals of apatite, a species of calcium phosphate with their crystal orientations aligned. This arrangement produces a fine structure possessing both strength and flexibility. Teeth are also assemblies of single apatite crystals, and enamel in particular is a high-hardness tissue comprised of densely packed fine apatite with an extremely high degree of crystallinity. Another example of biomineralization is the pearl layer of the Akoya pearl oyster, in which single crystals of aragonite, a calcium carbonate, are packed in an orderly fashion within a microscopic space. The proteins that fill in the surrounding gaps contribute to the creation of a beautiful sheen.

While biomineralization can occur in mild environments under normal temperatures and pressures, it is difficult to directly form the groups of inorganic crystals seen in hard tissues such as teeth, bone, and shells from simple solutions under normal temperature and pressure while maintaining high crystallinity. The mechanism used by organisms to build the tissues necessary for survival—the use of organic substances as templates—enables crystallization with lower activation energy. The application of this mechanism to industrial crystallization, which is totally unrelated to living organisms, is a promising area of research. Crystallization that utilizes organic–inorganic interaction processes in a mild environmental field not related to living organisms is commonly called “biomineralization-mimicking” or “biomineralization-based” crystallization.

Although biomineralization beneficially forms tissues necessary for maintaining normal organism function, it also produces substances that adversely affect organism health. For example, (broadly defined) biomineralization can cause gout, gallstones, kidney stones, urinary tract stones, vein wall deposit, and cholesterol accumulation in humans. Stones contain organic substances such as uric acid and urate salts, in addition to inorganic substances such as calcium phosphate and calcium oxalate salts. A cholesterol crystal, for example, is a natural organic substance. This means that the production of organic crystals on organic substance templates can be regarded as a type of biomineralization. Many of the crystals formed by biomineralization inside organisms, especially within the human body,

are calcium salts, so their formation can be generically classified as calcification. Representative examples of beneficial calcification include the formation of teeth and bone, while harmful calcification includes, in addition to stone formation, the buildup of atherosclerotic plaques, the calcification of brain tissue, and the accumulation of fine calcium salt crystals that often accompanies the presence of cancerous tissues.

Among the calcium salts formed by biomineralization, calcium phosphates, represented by apatite, have by far received the most attention and in-depth study. This is probably because calcium phosphate salts are not only integral to tissue formation but are also believed to be very deeply involved in life processes and in the evolution of species [1]. While there have been many debates on this topic, a consensus of opinions has not yet been reached. For instance, one enduring question is why vertebrates, as represented by humans, use apatite (a calcium phosphate salt) to produce hard tissues in the body while invertebrates such as shellfish use calcium carbonate salts such as aragonite and calcite to produce hard tissues. One explanation is that invertebrates have a unique immune mechanism. And while there are intriguing theories related to apatite and the origins of life, the supporting evidence is inconclusive. For example, the surface of apatite has extremely strong affinity for the substances constituting living organisms such as amino acids, proteins, sugars, and lipids. Moreover, amino acids arrange themselves with high regularity on apatite surfaces and are able to initiate condensation reactions, a key factor in the origin of life [2].

Biomineralization is a typical interdisciplinary topic that is related to physics, chemistry, and biology (including medical science), and the subject of interest depends on the perspective taken. When considered from the viewpoint of crystal growth, the important points are likely to include the growth mechanisms of biominerals themselves, the actual nature of the organic–inorganic interactions that are the essence of the biomineralization process, and the products in the environment with a complex chemical composition such as organisms.

As an example of biomineralization, these sections will describe and explain calcium phosphate salts—the most important biominerals in humans—with particular focus on apatite. In this chapter, the mechanisms of apatite crystal growth will be introduced. Apatite will be considered as purely an inorganic material, and developments in the understanding of crystal growth mechanisms in simple solution systems will be reviewed. In Chap. 4, examples of research focusing on the relationship between proteins and apatite will be described from the perspective of organic–inorganic interactions. The process used by proteins to control the formation of minerals will be explained, and the control of biomineralization using protein engineering will be described. In Chap. 5, the current state of research on the tooth enamel, as a representative example of biomineralization within an organism, will be reviewed. The relationship between the concept of apatite formation mechanisms with clusters as growth units (described in this chapter) and the roles of amorphous calcium phosphate (ACP) and octacalcium phosphate in the formation of enamel, which is attracting much attention, will be described.

3.2 Types and Solubilities of Calcium Phosphates

Phosphate ions, which comprise a phosphorous ion with a charge of +5 and an oxygen ion with a charge of -2, are grouped on the basis of their chemical composition into orthophosphates, metaphosphates, pyrophosphates, and polyphosphates. The phosphate ions described in the present chapter belong to the orthophosphate group. Orthophosphate ions, which have the chemical composition PO_4^{3-} , are a component of all the calcium phosphates that are described.

One of the characteristics of biomineralization is the variety of chemical compositions and crystal structures of the substances produced. Calcium phosphate is considered to be a representative biomineralization compound. Primary substances that are a calcium phosphate with a known chemical composition and structure and which can be precipitated as crystals between room temperature (about 25°C) and human body temperature (about 37°C) are dicalcium phosphate dihydrate (DCPD: $\text{CaHPO}_4 \cdot 2\text{H}_2\text{O}$), dicalcium phosphate anhydrous (DCPA: CaHPO_4), β -tricalcium phosphate (β -TCP: $\beta\text{-Ca}_3(\text{PO}_4)_2$), octacalcium phosphate (OCP: $\text{Ca}_8(\text{HPO}_4)_2(\text{PO}_4)_4 \cdot 5\text{H}_2\text{O}$), and hydroxyapatite (HAP: $\text{Ca}_{10}(\text{PO}_4)_6(\text{OH})_2$) [3,4]. In addition, while it does not itself form a crystal structure, one of the main precipitates is ACP. The following two paragraphs will briefly explain HAP and ACP, which are covered primarily in the present chapter, as well as the solubility of calcium phosphate salts. A recent detailed review of ACP can be found elsewhere [5].

In some instances, the crystal structure of HAP takes on the monoclinic system ($P2_1/b$) [6], while in others it takes on the hexagonal system ($P6_3/m$) [7]. The monoclinic structure is considered to be stable; however, the HAP in organisms has a hexagonal structure. The unit cell constants of HAP with hexagonal system are $a = b = 0.94302$, $c = 0.68911$ nm, and $\gamma = 120^\circ$, while the monoclinic HAP has a symmetry in which the length of the b -axis is twice that of the a -axis, with $a = 0.98421$, $b = 2a$, $c = 0.68814$ nm, and $\gamma = 120^\circ$ [8]. Structural analysis using synchrotron radiation has shown that the b -axis is slightly longer than $2a$ [9]. Although the stoichiometric composition of HAP is $\text{Ca}_{10}(\text{PO}_4)_6(\text{OH})_2$, hexagonal HAP with this composition is not found in the human body. HAP substitutes various ions within its core structure, so its chemical composition varies widely (for example, [3]). The CO_3^{2-} can substitute for PO_4^{3-} and a proportion of the OH^- groups, and F^- and Cl^- can substitute for a proportion of the OH^- groups. The substitution of CO_3^{2-} in HAP, which constitutes bone and teeth, is particularly common. It is generally thought that HAP in bone and teeth contains 4–5 wt.% and 3–5 wt.% carbon dioxide, respectively [10,11]; this HAP is sometimes referred to as carbonate-containing HAP. The channels created by Ca^{2+} in a crystal structure form a channel parallel to the c -axis, and the separation of ions from the channel and substitution of different ionic species readily occur. Instances are known in which gaps created by the separation of Ca^{2+} are replaced by cations such as Na^+ , Sr^{2+} , and Mg^{2+} . In these cases, a large stoichiometric discrepancy occurs, resulting in Ca-deficient HAP. The HAP in bone is a classic Ca-deficient HAP in which the Ca/P ratio does not attain the stoichiometric 1.67 value. When the calcium content

is the lowest, the Ca/P ratio may on occasion fall to around 1.50. In this chapter, the various species of HAP, including those with modified chemical compositions, are generically referred to as HAP unless otherwise noted.

Although ACP and amorphous HAP are clearly distinguishable, their structures have many similar features [12]. ACP readily forms under high-pH and high-supersaturation conditions, and its component ratios of calcium and phosphate vary over a range wider than that of HAP, depending on the environmental conditions and post-precipitation treatment. Early studies showed the Ca/P ratio to be 1.50 (with $\text{Ca}_3(\text{PO}_4)_2 \cdot x\text{H}_2\text{O}$ as a representative formula) [12–14]. Subsequent studies showed that the Ca/P ratio can be changed from 1.18 to 1.50 by varying the pH range from 6.6 to 10.6 and that sufficient rinsing after precipitation stabilizes the ratio at 1.50 [15]. Instances have been reported in which the Ca/P ratio was increased to 2.50 by using an even higher pH (~11.7) [16]. There are also reports describing ACP species with the same chemical composition that can exist in two phases (ACP1 and ACP2) differing in solubility [17,18]. ACP1 is regarded as closer to a crystalline state than ACP2, and while both phases are amorphous, this may contrast with differences in the crystals' polymorphic structure. Within its structure, ACP contains 10–20 wt. % water molecules, which separate from the structure due to an increase in temperature. ACP has an essentially “loose” structure; however, the arrangement of constituent ions is not completely random. Nano-sized orderly structures (clusters) are linked with one another through weak bonds. The Posner cluster, $\text{Ca}_9(\text{PO}_4)_6$, is a representative example of this model [19]. Water molecules fill the gaps between these clusters. The result of ^{31}P nuclear magnetic resonance (NMR) measurements of ACP indicated that the strength of the ACP sidebands is a characteristic structural distortion of unprotonated phosphate (not of a mixture of it and protonated phosphates) [20]. X-ray diffraction analysis of ACP revealed that it has amorphous properties (broad diffraction patterns). However, extended X-ray adsorption fine structure (EXAFS) analysis showed that its structure is characterized by a short-range order similar to that of HAP [21–23]. These results suggest that ACP and HAP essentially have a common minimal structural unit. Observations of the phase transformation process from ACP to HAP using time-resolved static light scattering have shown that ACP can structurally transform directly into HAP without dissolution [24]. Assuming no similarities between the minimal structural units of ACP and HAP, the energy needed for directly transforming one structure into the other should be extraordinarily large. It is natural, therefore, to consider that ACP and HAP share a common structural unit.

Figure 3.1a shows the solubility curve (37°C) of each calcium phosphate salt in the $\text{Ca}(\text{OH})_2\text{-H}_3\text{PO}_4\text{-H}_2\text{O}$ system. The solubility product of each calcium phosphate was presented in a review article [4]. Since the standard pH of human body fluid is 7.2–7.4, HAP has the lowest solubility and the most stable phase under physiological conditions. This means that metastable calcium phosphates other than HAP that precipitate in an aqueous solution with a near-neutral pH are likely to transform into HAP in a time-dependent manner unless the solution pH changes. The solubility of HAP fluctuates with the ionic species in its structure. In particular, the substitution of CO_3^{2-} increases the HAP solubility although a consensus has not

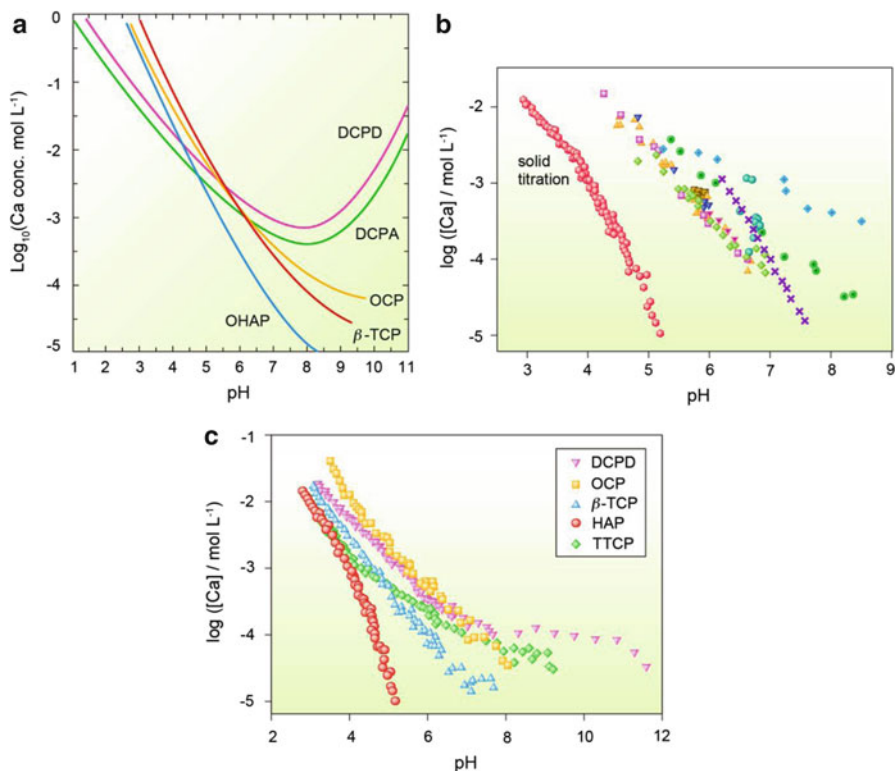


Fig. 3.1 (a) Solubility isotherms of calcium phosphate minerals in the system $\text{Ca}(\text{OH})_2\text{-H}_3\text{PO}_4\text{-H}_2\text{O}$ at 37°C (reproduced with permission from [3]) (copyright 1994, Elsevier). (b) Solubility of HAP by solid titration method compared with conventional excess-solid method. References of data in conventional method can be seen in original article [25]. (c) Solid titration isotherms for calcium phosphates salts (reproduced with permission from ref. [25]) (copyright 2009, American Chemical Society)

been reached regarding changes in the solubility product. One reason for this may be that solubility measurements are not performed under standardized conditions since the solubility of the solid phase is affected by the strain introduced into the structure by ionic substitution and the CO_3^{2-} content in the environmental field (solution phase). The concentrations of calcium and phosphate ions contained in human body fluid are naturally in a supersaturated state with respect to HAP. Nonetheless, indiscriminate precipitation of HAP does not occur in the human body. One reason for this is that high concentrations of CO_2 dissolve into the body fluids and become a carbonate buffer, thereby raising the solubility of HAP.

The solubility of fluorapatite ($\text{Ca}_{10}(\text{PO}_4)_6\text{F}_2$), in which the OH^- of HAP is completely replaced by F^- , is lower than that of HAP. Within the HAP structure, there is a column of OH^- groups parallel to the c -axis. However, since the position of each OH^- is slightly staggered relative to the others, there is strain in the

structure. Replacing the OH^- with F^- is thought to release the strain so that the subsequent stabilization of the crystal structure reduces the solubility of the solid phase. Another likely cause of structural stabilization is that the replacement of the polar group OH^- by the nonpolar group F^- affects the local charge balance. The solubility of ACP is not shown in Fig. 3.1a. However, as mentioned above, the phase transformation from ACP to HAP has been observed. Therefore, at least near a neutral pH, ACP has a higher solubility than HAP. Although the solubility of all calcium phosphates rapidly increases with decreasing pH, the rate of increase differs greatly depending on the type of salt. Compared to HAP, OCP, and TCP, the pH-dependence of solubility for DCPA and DCPD is relatively small. For this reason, the solubility of HAP exceeds that of DCPA at $\text{pH} \leq 4.5$, and DCPA becomes the most stable phase. The form of the solubility curves for each calcium phosphate in Fig. 3.1a, as well as the pH at which DCPA becomes the most stable phase, vary to some extent when there are ionic species other than calcium and phosphoric acid in the solution. However, it is thought that HAP is the most stable at a near-neutral pH and that DCPA or DCPD is the most stable at a low pH. However, questions have been raised that challenge this idea [25].

The conventional method for measuring solubility is to inject an excess amount of the solid phase of the target calcium phosphate salt into solution, and after sufficient stirring, measure the ionic concentrations and calculate the equilibrium concentrations. Pan and Darvell pointed out a shortcoming in this method—solid calcium phosphate in solution undergoes incongruent dissolution, which in turn triggers a phase transformation that results in large errors in the calculated equilibrium concentrations. They measured the solubility of HAP using a unique solid-titration method and found that it was considerably lower than conventionally reported values (Fig. 3.1b). They also measured the solubility of other calcium phosphate salts using the solid-titration method and compared the results. They concluded that HAP represented the most stable phase for $\text{pH} \leq 4.2$ and not DCPD, as was generally believed (Fig. 3.1c). In explaining why DCPD was believed to be the most stable phase, they mentioned the stability of DCPD and the nucleation frequency and concluded that DCPD is far more likely to nucleate than HAP at low pH. In titration experiments using solid DCPD, the only phase observed at a pH of 3.60 or 4.50 was DCPD; however, when a minute amount of HAP was added to this equilibrium state, the DCPD disappeared and highly crystalline HAP formed at a pH of 3.30, 3.60, and 4.47.

3.3 Crystal Growth Mechanisms in an Aqueous Solution System: Historical Review

Given that the growth of HAP occurs in an aqueous solution environment, the history of research on the mechanisms of crystal growth in aqueous solutions will be reviewed before the growth mechanisms of HAP are discussed.

Theoretical treatment of crystal growth mechanisms in dilute environments at the atomic scale was given in the form of the Burton-Cabrera-Frank (BCF) model in 1951 [26]. The growth rate of crystal face R in which the growth unit goes through the surface diffusion before incorporating in the growth step is expressed as a function of the driving force of growth (supersaturation, σ):

$$R = C \frac{\sigma^2}{\sigma_1} \tanh \frac{\sigma_1}{\sigma}, \quad (3.1)$$

where C and σ_1 are constants determined by the growth conditions. A characteristic of this formula is that it is possible to approximate $R \sim \sigma^2$ at low supersaturation and $R \sim \sigma$ at high supersaturation, which was frequently used for discussing the growth mechanisms.

The research conducted on NaClO_3 is an example in which detailed analysis of growth mechanism using the BCF model was performed on crystal grown from aqueous solution [27]. The relationship between the face growth rates and supersaturation was investigated with precise temperature control ($<1/100^\circ\text{C}$ of fluctuation) at low supersaturation ($\leq 1\%$), and the data were analyzed using (3.1). It was concluded that spiral growth via surface diffusion occurred. This was the first time that spiral growth via surface diffusion in aqueous solution was quantitatively shown. Denk and Botsaris performed the measurements of potassium alum (K-Alum) under high-supersaturation conditions and concluded that the data could be interpreted by considering the combination of spiral growth and two-dimensional nucleation [28]. Subsequently, growth mechanisms approximated using face growth rate data and growth theory equations became widely used, and the growth mechanisms of numerous aqueous inorganic and organic crystals were elucidated (for example, [29]).

These studies focused on two important topics. The first was the growth mode in an aqueous solution system (spiral or two-dimensional nucleation growth), and the second was the investigation of the rate-limiting process of growth, in which emphasis was placed on the assertion that the importance of surface diffusion that had originally been applied to crystals grown in the gas system also holds for aqueous solution systems. Chernov proposed a model in which the growth unit is directly incorporated from the environmental phase into growth steps [30]. This model showed that the surface diffusion of the growth unit is not important in a solution system, particularly an aqueous solution system.

Following the tests of the spiral growth model by measuring the crystal growth rate, attempts to obtain direct evidence for spiral growth from surface observations were actively conducted from the 1970s onward, even for aqueous solution crystals. Examples include the observations of NaCl and KCl [31], K-Alum [32], potassium hydrogen phthalate (KAP) [33], and $\text{NiSO}_4 \cdot 6\text{H}_2\text{O}$ [34].

In a study of crystal growth mechanisms, van Erk et al. vividly showed the importance of surface observations although not in regard to crystals grown in aqueous solutions. They measured the growth rate of garnet crystals grown by liquid phase epitaxy and concluded that spiral growth through surface diffusion had

occurred [35]. Using surface observations conducted, and after performing detailed measurement of the slope of the growth hillock formed by spiral steps, together with face growth rate data, they indirectly calculated the step velocity. It disagreed with the linear dependence on supersaturation predicted by the BCF model. They explained this contradiction by arguing that the step velocity increased non-linearly due to two-dimensional nucleation occurring at the terraces between steps.

With spiral growth, the original BCF model described the face growth rate on the basis of the behavior of the growth steps at a single growth center on the crystal surface. However, there are multiple growth centers on a crystal surface, and the ones that control the growth rate undergo changes as a result of alterations in their relative activity that are associated with supersaturation. Efforts to resolve this problem and conduct measurements near the theoretically assumed growth conditions were carried out vigorously from the late 1980s to the early 1990s using *in situ* optical interferometry. This method was applied to ADP and KDP crystals [36,37] and subsequently led to studies on $\text{Ba}(\text{NO}_3)_2$ [38] and on K-Alum [39].

The use of interferometry for studying various soluble inorganic crystals has clarified many phenomena. For example, observations of KDP and K-Alum confirmed the nonlinear dependence of the step velocity on supersaturation, which was similar with that reported by van Erk et al. for the garnet crystal. However, it was shown that this nonlinear dependence is not due to two-dimensional nucleation at the terraces but rather to a decrease in velocity caused by adsorption of impurities on the step front at low supersaturation and a rapid increase in velocity caused by less adsorption of impurities with an increase in supersaturation. It was also shown that step behavior, which differs from that predicted by the BCF model, greatly affects the dependence of the face growth rate on the supersaturation. For example, even when spiral growth occurs on a crystal surface, the relationship between the growth rate and supersaturation could suggest growth by two-dimensional nucleation. These findings revealed the danger inherent in the simplistic fitting of growth rate data to a model.

The rate-limiting process of growth has also been investigated using interferometry. In early research on KDP and ADP, surface diffusion was thought to be unimportant, as it was for research on $\text{Ba}(\text{NO}_3)_2$ and K-Alum. For crystal growth in an aqueous solution system, the consensus was that surface diffusion did not play a major role, and even if it were present, the diffusion length would be minimal. Vekilov et al. investigated the previously unobserved faces of ADP crystals and, after performing detailed comparison of data using growth models, concluded that growth progressed via surface diffusion and that a surface kinetic process including surface diffusion was rate-limiting [40]. It is currently understood that, even in the same crystal, the optimal growth model depends on the relative importance of each elemental process for each crystal face.

Observations using interferometry of two-dimensional nucleation of ADP have been performed [41]. The observations and subsequent quantitative analysis revealed that impurities reduce the activation energy needed for nucleation at low supersaturation and are active sites for heterogeneous nucleation. Homogeneous nucleation takes place only at high supersaturation. This has been verified by the

finding that the edge free energy required for nucleation is discontinuously smaller at low supersaturation. As will be discussed later, even for HAP growth, there are cases in which discrepancies between edge-free-energy data sets can be explained by considering a heterogeneous nucleation model.

3.4 HAP Crystal Growth Mechanisms

3.4.1 Driving Force for Growth

In a two-component simple aqueous solution system of soluble salts, supersaturation—the thermodynamic driving force for growth—is determined by the solubility curve of the solid phase. This method is sufficiently useful as an approximation; there are no significant problems even when interpreting data on growth rate versus supersaturation and in calculating physical constants related to growth. However, in the case of insoluble calcium phosphate salts, including HAP, there are three problems in particular: the possibility of multistep dissociation equilibrium of the phosphate group in solution, the possibility of ion pair formation between calcium and phosphate ions, and the possibility that the solutions in which the crystals are grown contains cations and anions other than calcium and phosphate. For these reasons, the driving force is normally defined using the ion product I_p —defined as the ionic strength I calculated from the concentration and the total charge of each ion in the solution—and the solubility product of the solid phase K_{sp} (solely a function of temperature).

Let a_i and c_i be the activity and concentration, respectively, of the i th ion contained in the solution.

$$a_i = f_{\pm} c_i, \quad (3.2)$$

where f_{\pm} is the mean activity coefficient, which, from the Debye–Hückel approximation, is expressed by the following equations using ionic strength I :

$$\log f_{\pm} = \frac{-Az_i^2\sqrt{I}}{1 + Br_i\sqrt{I}} \quad (3.3)$$

$$I = 0.5 \sum c_i z_i^2. \quad (3.4)$$

The z_i is the charge of the i th ion, r_i is the effective radius of each ion, and A and B are theoretical coefficients determined by the specific permittivity of solvent ϵ_r and absolute temperature T , commonly using

$$A = \frac{1.8246 \times 10^6}{(\epsilon_r T)^{3/2}} \quad (3.5)$$

$$B = \frac{50.29 \times 10^8}{(\varepsilon_r T)^{1/2}}. \quad (3.6)$$

The driving force for growth, i.e., the chemical potential difference between the solid phase and liquid phase $\Delta\mu$, is

$$\frac{\Delta\mu}{kT} = \ln \frac{a_i}{a_{ei}} = \ln \frac{I_P}{K_{sp}}, \quad (3.7)$$

where a_{ei} is the ionic activity at equilibrium. Between $\Delta\mu$ and supersaturation σ , the relationship $\Delta\mu/kT = \ln(1 + \sigma)$ holds. Therefore,

$$\sigma = \frac{I_P}{K_{sp}} - 1. \quad (3.8)$$

However, to enable comparisons under a consistent supersaturation, even between solid phases that have naturally different stoichiometric ratios, an equation standardized by N , the sum of the valences for each ion comprising the solid phase, is used [42]:

$$\sigma = \left(\frac{I_P}{K_{sp}} \right)^{1/N} - 1. \quad (3.9)$$

For $\text{Ca}_{10}(\text{PO}_4)_6(\text{OH})_2$, which is the stoichiometric composition of HAP, N is 18. In the form of (3.9), a constant supersaturation is applied even if the descriptive formula for the chemical composition of the target solid phase differs. For HAP, K_{sp} is occasionally defined on the basis of its half-unit cell $\text{Ca}_5(\text{PO}_4)_3\text{OH}$. However, this value turns out to be approximately the square root of the K_{sp} value for $\text{Ca}_{10}(\text{PO}_4)_6(\text{OH})_2$, the corresponding full-unit cell. Therefore, supersaturation calculated using (3.9) is the same value independent of the definition of the unit cell.

Equation (3.9) includes an ionic product term. For this reason, even if the calcium or phosphate concentrations are constant, the supersaturation greatly varies depending on the background salt concentration, and this affects the conditions for growth and phase transformation. For example, the structural reconstruction-type phase transformation of ACP to HAP, which is described elsewhere [24], occurs when only calcium and phosphate ions (excluding hydrogen and hydroxide ions) are contained in the solution. When the supersaturation is raised by adding 10 mM of KCl to this solution, the phase transformation switches to a heterogeneous-type nucleation in which HAP forms around ACP as the nucleus (or template).

3.4.2 Biological HAP Formation Model

The HAP growth mechanisms, including nucleation, differ considerably depending on whether they are viewed from a biological or a physicochemical perspective.

With HAP, which forms bone tissue in the human body, a number of formation theories were proposed many years ago. For example, Robinson theorized that HAP nucleation occurs as a result of a localized increase in the phosphate ion concentration due to hydrolysis of the organic phosphate ester substrate by the enzyme alkaline phosphatase [43]. Newman and Newman theorized that the molecular chains on the collagen surfaces behave as effective sites of HAP nucleation [1]. Brighton and Hunt theorized which that once the fine HAP nuclei formed from the calcium and phosphate ions in a matrix vesicle grow to a certain size, they break through and arrange themselves on the collagen fibers [44]. Newman and Newman's epitaxial theory leads to the contemporary notion of biomineralization. With the matrix vesicle theory, the amount of HAP that can be formed in the bone is much greater than the amount that can be formed in the matrix vesicles. In other words, in addition to the HAP that is formed within the matrix vesicles, there is a need for HAP formation to occur directly from the body fluids onto collagen fibers.

Each of these theories focuses on HAP nucleation. The growth and dissolution behavior of HAP in formed bone tissue has led to a biological consensus on the concept of remodeling [45]: the renewal over time of bone tissue occurs through the growth and dissolution of HAP. It involves competition between osteoclasts, which dissolve bone, and osteoblasts, which create bone.

3.4.3 Constant Composition Method

Consideration of HAP as a pure inorganic compound in an attempt to understand its mechanisms of growth and dissolution physicochemically would not reveal the essence of these mechanisms due to the complex systems—including cells—that are involved. Even considering that various types of cells play a primary role in bone tissue formation within the organism, the phenomenon that consequently occurs at the interface between HAP and the environmental phase (body fluid) is ultimately crystal growth of inorganic salts. Therefore, illustration of the HAP formation mechanisms within the organism requires first conducting studies in simple cell-free aqueous solution systems. Researchers investigating the HAP growth mechanisms have mainly been doing this since the 1970s.

Early studies were done using Bennema's procedure: estimate the dependence of the HAP growth rate on supersaturation and compare the data with growth theories such as the BCF model to elucidate the growth mechanisms. In a growth experiment using highly crystalline synthetic HAP polycrystals as seeds [46], the growth rate and chemical composition of HAP were obtained by measuring the solution pH as well as the calcium and phosphate ion concentrations accompanying growth. The growth rate was estimated from the change in solution composition, which was derived from HAP surface area. The growth rate data had a relationship of $R \sim \sigma^2$, and it was concluded that spiral growth, which could be expected in solutions with low supersaturation, took place. Since the measurements were in a closed system, the change in the chemical composition of the solution associated with HAP growth would lead to a change in supersaturation. In addition, it could not be conclusively

stated that the chemical composition of the formed HAP was constant throughout, and it was necessary to carefully analyze errors in the rate data since the amount of growth was small. Nonetheless, this study showed the possibility of investigating growth mechanisms even for insoluble salts using a method similar to that used for soluble salts.

Development of the constant composition (CC) method [47] ultimately resolved the technical problems of the experiment discussed above. In this method, real-time measurements of the pH and chemical composition of the growth solution are taken with a glass electrode. The composition of the mixture is maintained by automatically supplementing the solution with drops containing calcium or phosphate ions. In order to maintain the lowered pH at its original value during growth, a solution containing hydroxide ions is added. The growth rate is calculated from the surface area of the seed crystal and the drip rate. The CC method has three particular advantages: (1) more accurate growth rate data can be obtained since it is possible to sufficiently grow the crystals with respect to the seeds, (2) the amount of growth can be measured even in solutions with a relatively low supersaturation since the measurement of the pH and chemical composition with the glass electrode is highly sensitive, and (3) the metastable phase that forms during HAP growth can be estimated by tracking changes in the solution composition. The CC method has been used to not only measure the growth rate but also the dissolution rate and nucleation induction time.

In the CC method, the relationship between the growth rate and supersaturation is approximated by the following simple equation, and the growth mechanisms are discussed in terms of n :

$$R = C \sigma^n \quad (C \text{ is the reaction constant : } n \text{ is the reaction order.) \quad (3.10)$$

Koutsoukos et al. grew HAP to an amount several times that of the seed crystal using the CC method and obtained the relationship $R \sim \sigma$ [48]. From this result they concluded that spiral growth is involved in HAP growth. A similar conclusion was reached in other studies [49]. In contrast, Arends et al. obtained the relationship $R \sim \sigma^{2.9-3.2}$, and postulated that growth involved multiple two-dimensional nucleation [50]. Christoffersen and Christoffersen used various growth theory equations to analyze HAP growth rate data obtained with the CC method. They concluded that while growth rate equation that takes multiple two-dimensional nucleation into account is optimal, spiral growth occurring simultaneously with two-dimensional nucleation would be possible [51,52]. Although debates on growth mechanisms are common, with the CC method, there are also debates ranging from the reaction orders to growth path (via surface diffusion or not).

3.4.4 *Synthesis of HAP Single Crystal*

Although it is desirable to conduct growth rate measurements for each crystal face using a single crystal when investigating crystal growth mechanisms in relation to

theory, this type of research for HAP is uncommon. This is not due to technical hurdles that prevent the growth of a single crystal to a size suitable for handling. Indeed, in the 1950s and 1960s, there were numerous investigations of the synthesis of HAP single crystals using the hydrothermal method. With early hydrothermal synthesis methods, the starting material was placed in a sealed container, and synthesis was performed across several days at a temperature of 300–700°C under high pressure (8.6–200 MPa). The type of starting material and synthesis steps varied widely. The approaches included recrystallizing HAP polycrystal in NaOH solution [53,54], hydrolyzing calcium phosphate salts [55], mixing CaO and β -Ca₂P₂O₇ stoichiometrically and reacting them in an aqueous solution [56], and using reactions in a Ca(NO₃)₂-KH₂PO₄-NaOH-H₂O system [57]. In later studies, simple methods of recrystallizing HAP polycrystal in pure water [58], as well as methods using reactions in an H₃PO₄-Ca(NO₃)₂-H₂O system [59], were used. One successful example of promoting the growth of HAP single crystals by hydrothermal synthesis resulted in synthesis of a giant crystal (7 × 3 × 3 mm) [60].

Synthesis of HAP using a chemical composition containing CO₃²⁻, similar to that found in organisms, has also been carried out. Studies using recrystallization of HAP polycrystal have produced HAP single crystals about 0.5 mm in length after 3 months under conditions of 300°C and a CO₂ partial pressure of 16.7 MPa [61]. This single crystal had a hexagonal columnar morphology consisting of a (10 $\bar{1}$ 0) prism face (*a*-face), a (10 $\bar{1}$ 1) face, and a (0001) basal face (*c*-face). When the CO₃²⁻ group was substituted for the OH⁻ group and the CO₃²⁻ content was increased slightly to above 0.1 wt.%, the *c*-face incidence increased. An experiment using hydrolysis of CaHPO₄ in the presence of CO₂ gas resulted in a giant HAP single crystal (length of 12 mm (*c*-axis direction) and width of 0.2 mm) [62]. In this experiment, dry ice was added to the aqueous solution as a CO₃²⁻ source, and a top-down temperature gradient was applied using long cylindrical synthesis container to generate convections. HAP single crystals nucleated on the sintered bodies of synthetic HAP suspended in the solution, taking the morphology of a hexagonal column with a large aspect ratio consisting of *a*- and *c*-faces. As in the previous case, the CO₃²⁻ group was substituted for the OH group, and its content was 0.09–0.65 wt.%. The Ca/P ratio of the grown HAP crystals was 1.60–1.67.

Large crystals are easier to obtain with the flux method than with the hydrothermal synthesis method. In one experiment, for example, cooling a flux in which TCP was dissolved in a Ca(OH)₂ melt resulted in the growth of a HAP crystal 4–8 mm long in the *c*-axis direction and 0.5 mm wide [63]. In this experiment, 10 wt.% TCP and 90 wt.% Ca(OH)₂ were used. The flux was maintained at 925°C for 24 h, and then the crystal was grown by gradually cooling the flux over several days to 775°C, followed by rapid cooling to room temperature. The obtained crystal was a monoclinic HAP. Observations of cross-sections cut perpendicular to the *c*-axis revealed a morphology approximating that of a twin crystal. Synthesis in which deuterium was substituted for the hydrogen in Ca(OH)₂ was also performed and the resulting HAP crystals contained deuterium rather than hydrogen. A HAP crystal 8 mm long and 0.5 mm wide was also obtained using a similar method in which 25 wt.% water was added to the flux (hydrothermal flux) and the temperature was increased from 750 to 880°C to suppress unnecessary nucleation [64].

3.4.5 *Real-Time Phase-Shift Interferometry for Observation of Biomineral Growth*

Although it is possible in principle to obtain large HAP crystals that can be used for observation, the rate of growth for each face is not performed using a single HAP crystal due to the slowness of the growth. The growth rate of a soluble inorganic crystal depends on the type of crystal and crystal face. It typically ranges from 10 to 100 nm/s even when the supersaturation is a few percent. The growth rate of a HAP crystal is thought to be 2–4 orders of magnitude lower than this value. The simplest way to measure the growth rate using a single crystal is to measure the amount of normal growth of the target face. However, an excessively low growth rate markedly decreases the time resolution for the growth amount, and precise data to compare with theory cannot be obtained. Although optical interferometry can measure growth rates far more rapidly than simply measuring the normal growth of the crystal face, the technique is extremely sensitive to temperature changes in the vicinity of the equipment and to external disturbances such as vibration. It is therefore not well suited to measurements of long duration. For this reason, optical interferometry has not been applied to the measurement of HAP growth rates. However, real-time phase-shift interferometry has helped to resolve the problem of external disturbances [65].

Although real-time phase-shift interferometry is essentially a type of optical interferometry, in contrast to conventional interferometry, which produces only an interference image of the crystal surface, it simultaneously (or nearly simultaneously) obtains multiple interference images that are slightly phase shifted from each other. This method markedly improves the height resolution because it includes calculation of the two-dimensional intensity-distribution profile using multiple interference images. This enables the increments in the height direction to be observed within a short time. Since low-frequency external disturbances are the primary factor that causes artifactual changes in interference fringes, the phase-shift method can greatly reduce the effects of these disturbances. While the height resolution depends on the number of interference images used, phase-shift interferometry can increase the height resolution to more than 100 times that of conventional two-beam interferometry, which is comparable to the resolution achieved using atomic force microscopy (AFM).

The first application of phase-shift interferometry to biominerals was to calcite [66]. With natural calcite crystals as the seed, the dissolution rate in aqueous solution was measured in situ. Maruyama et al. elucidated the growth process of calcite [67]. Their research included detailed investigation of how the chirality of amino acids (asparagines), included as an impurity, affected the step velocity. The calcite growth rate was estimated with good precision by taking measurements over approximately 20 min.

HAP growth rate measurements using the phase-shift method were first reported for the *c*-face of HAP [68]. An example of *c*-face observation using real-time phase-shift interferometry is shown in Fig.3.2. In this research using large HAP single crystals obtained from hydrothermal synthesis as seeds, a pseudo body fluid

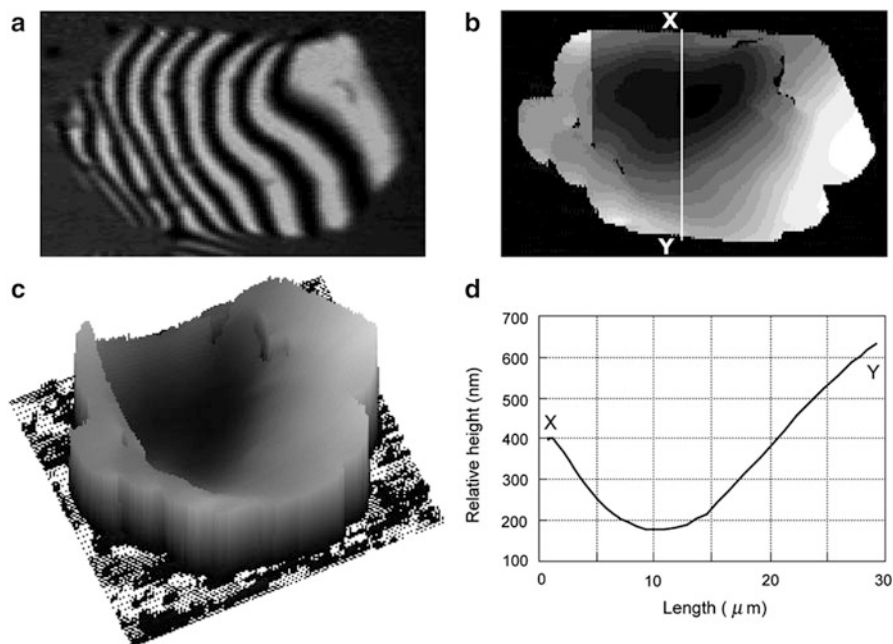


Fig. 3.2 Observation of HAP *c*-face using Moire phase-shift interferometry. (a) Original interferogram of *c*-face. (b) Two-dimensional phase distribution profile produced using three interferograms with phase-shifted 90° each other. (c) Three-dimensional surface image created using (b). (d) Section profile between X and Y in (b) (reproduced with permission from [68]) (copyright 1998, American Chemical Society)

mimicking the components of human body fluid was used as the supersaturated solution in which the HAP was grown. The concentrations of NaCl, calcium ion, and phosphate ion, as well as the pH, of the pseudo body fluid were adjusted to simulate those found in human body fluid. Several unique contrivances were devised for the interferometers used for the growth rate measurements. For example, to completely exclude fluctuations in the interference fringes due to external disturbances, a “common-path” interferometer was constructed using a Nomarski prism in which the test and reference optical paths in the interferometer pass through nearly identical paths. In principle, a common-path type interferometer is completely unaffected by disturbances since any disturbance acts identically on the test and reference optical paths. However, fluctuations in the interference fringes due to movement of the crystal itself cannot be removed. Even if the crystal is immobilized using an adhesive agent with a low expansion rate, the position of the crystal undergoes very slight irregular fluctuations over an extended period of time. Therefore, for the *a*-face, for which the growth rate is more than an order of magnitude lower than that for the *c*-face, growth rate measurements even with phase-shift interferometry have not succeeded.

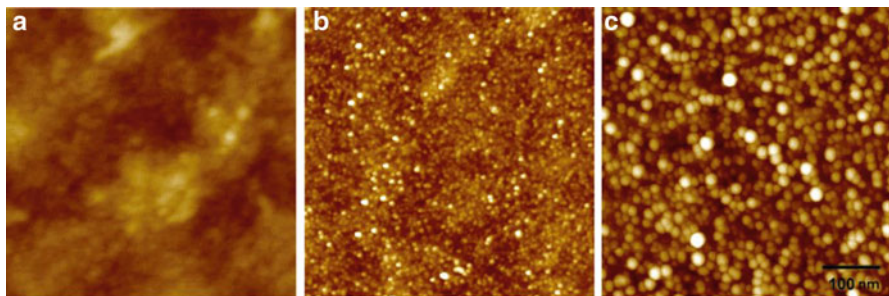


Fig. 3.3 AFM images of HAP *c*-face growing in pseudo-body fluid. (a) Original seed surface. (b) Surface after 5 min of growth. Many small islands grew. (c) Surface after 2 h of growth. Number and size of islands increased. Growth proceeded by multiple two-dimensional nucleation (reproduced with permission from [69]) (copyright 1998, American Chemical Society)

3.4.6 Analysis of Growth Features and Growth Rate Data of HAP *c*-face

The importance of surface observations in the investigation of growth mechanisms was described above. While surface observation is clearly possible with phase-shift interferometry, the resolution in the within-plane horizontal direction is limited to that at the normal optical microscopic level although that in the height direction is superior. For this reason, detailed surface observations of the HAP *c*-face using AFM were performed in combination with the growth rate measurements using the phase-shift interferometry. While AFM observations are not in situ, they are able to give a clear picture of the growth mode of the *c*-face in pseudo-body fluid.

Results of such observations are shown in Fig. 3.3, [69]. The crystal was grown for 5 min in pseudo body fluid followed by removal and observation with AFM (Fig. 3.3b). Innumerable small islands had formed on the surface. After observation, the crystal was returned to the pseudo body fluid and grown for an additional 2 h. The number and the size of the islands greatly increased, as shown in Fig. 3.3c. The growth of the *c*-face therefore proceeds in a multiple two-dimensional nucleation mode. In this study, the lowest supersaturation in which growth was confirmed by AFM was $\sigma = 0.85$. However, growth was multiple two-dimensional nucleation even in this supersaturation, and no spiral growth was observed. The face growth rate via multiple two-dimensional nucleation is expressed by the formula below, with h as the height of the formed two-dimensional nucleus, v as the step velocity of the two-dimensional nucleus, and J as the frequency of two-dimensional nucleation [70]:

$$R = h(\pi v^2 J / 3)^{1/3} \quad (3.11)$$

$$v = \varpi C_e \beta \sigma \quad (3.12)$$

$$J = B \exp(-\pi \alpha^2 \varpi h / k_B T \Delta \mu) = B \exp\{-\pi \alpha^2 \varpi h / (k_B T)^2 \ln(1 + \sigma)\}. \quad (3.13)$$

The β in (3.12) is a physical quantity known as the step kinetic coefficient. It corresponds to the rate coefficient when a growth unit is incorporated into a step and is expressed as $\beta \sim \exp(-E/k_B T)$ using activation energy E for growth unit incorporation. The C_e is the equilibrium concentration. The α in (3.13) is the surface energy and is related to edge free energy γ on the step front: $\gamma = \alpha(h\varpi)^{1/2}$. The ϖ is the molecular volume of the crystal. Factor B is given by

$$B = Z(2\pi N C \varpi \gamma / \Delta\mu) \nu \exp(-E/k_B T). \quad (3.14)$$

where Z is the Zeldovich factor, and N and C are constants. Since $Z = (\Delta\mu)^{3/2} / 4\pi\gamma(k_B T)^{1/2}$,

$$B = 0.5N\varpi C\nu \exp(-E/k_B T)(1 + \sigma)\{\ln(1 + \sigma)\}^{1/2} \exp\{-\pi\gamma^2/(k_B T)^2 \ln(1 + \sigma)\}, \quad (3.15)$$

and ultimately the growth rate is given as

$$R = K\sigma^{2/3}(1 + \sigma)^{1/3}\{\ln(1 + \sigma)\}^{1/6} \exp[-\pi\gamma^2/\{3(k_B T)^2 \ln(1 + \sigma)\}]. \quad (3.16)$$

Here, K is a constant that includes E . Taking the logarithms on both sides of (3.16) gives

$$\ln[R/[\sigma^{2/3}(1 + \sigma)^{1/3}\{\ln(1 + \sigma)\}^{1/6}]] = \ln K - \{\pi\gamma^2/3(k_B T)^2\} \times 1/\ln(1 + \sigma). \quad (3.17)$$

Calculating the left side from the measured growth rate and plotting it against $1/\ln(1 + \sigma)$ gives the most important parameter for two-dimensional nucleation, γ . The value of γ for the c -face of the HAP crystal was determined to be $3.3 k_B T$. When surface energy α , calculated from growth rate measurements based on the CC method, is converted to γ , its value is estimated as $\gamma = 1.1 - 2.0 k_B T$, which is considerably smaller than $3.3 k_B T$. In the CC method, the growth crystal face is not specified; hence, there are problems with direct comparisons between the two values. However, assuming that the results of the CC method are representative of the γ value of the c -face makes it possible to explain the differences between the two in terms of the nucleation mode.

The growth rate has been measured using the phase-shift method for supersaturation ranging from 9.8 to 22.0. Although measurements have been performed below this range, the results were deemed unusable because of the large distribution of the data. In contrast, the supersaturation range used for measurements with the CC method was set to 0.4–7.0, which is considerably lower than for the phase-shift method. As seen in the two-dimensional nucleation of soluble inorganic crystals, heterogeneous nucleation with impurities as active sites is more likely to occur at low supersaturation, and the apparent γ markedly decreases. With HAP as well, for which heterogeneous nucleation occurs at low supersaturation and homogeneous

nucleation occurs at high supersaturation, it is possible to explain the above results. In fact, for measurements based on the phase-shift method, the growth rate data in the low supersaturation range (while highly variable) does not lie on the expected curve extrapolated from that in the high supersaturation range.

The effects of adding zinc or magnesium ions to the pseudo-body fluid have also been investigated for growth rate measurements of the *c*-face [71, 72]. Although both elements are essential for organisms, they are thought to be impurities for HAP growth [73–75]. AFM observations of *c*-face growth in a system containing 0.03–1.5 mM of magnesium ions or 0.3–7.5 μM of zinc ions added to pseudo-body fluid with $\sigma = 22.0$ revealed that they strongly inhibit the growth of the two-dimensional nucleus. The effect of zinc ions in particular is more pronounced than that of magnesium ions. The effects of magnesium and zinc ions on γ from data on growth rate measurements are carried out at various levels of supersaturation with their concentrations fixed at 0.06 mM and 0.75 μM , respectively. Liu et al. has formalized the growth rate for heterogeneous nucleation mode when impurities are present [76]:

$$R = C_2 \beta \sigma^{2/3} (1 + \sigma)^{1/3} \{\ln(1 + \sigma)\}^{1/6} \exp[-\pi \gamma_0^2 f / \{3(k_B T)^2 \ln(1 + \sigma)\}] \delta^{1/3} \quad (3.18)$$

$$\begin{aligned} \ln[R / \{\sigma^{2/3} (1 + \sigma)^{1/3} \{\ln(1 + \sigma)\}^{1/6}\}] &= \ln C_2 + \ln \beta - \{\pi \gamma_0^2 f / 3(k_B T)^2\} \\ &\times 1 / \ln(1 + \sigma) + \ln \delta^{1/3}. \end{aligned} \quad (3.19)$$

In (3.18), C_2 is a constant, and γ_0 is the edge free energy of a two-dimensional nucleus in a system in which impurities are absent. In (3.19), f and δ are physical quantities unique to heterogeneous nucleation: the former is the ratio of the radii of the critical two-dimensional nucleus to that of the impurity particles, and the latter is the contact angle between the two-dimensional nucleus and the impurity particles. Both f and δ have a range of $0 < f, \delta \leq 1$, and when $f = \delta = 1$, (3.18) coincides with (3.16), which indicates homogeneous nucleation. The function $\gamma_i = \gamma_0 \times f^{1/2}$ (i = impurity type) relates γ_0 to γ_i , the edge-free energy in the presence of impurities. Finally, $\gamma_0 = 3.3k_B T$, $\gamma_{\text{Mg}} = 3.0k_B T$, and $\gamma_{\text{Zn}} = 3.4k_B T$, and $f_{\text{Mg}} = 0.8$ and $f_{\text{Zn}} = 1.1$ were obtained. On the basis of the permissible range for f and the measurement error for γ , f_{Zn} can be regarded to be 1.0, meaning that the addition of zinc does not affect γ . Although the difference between the measured γ and that obtained in a pure solution was somewhat larger than the measurement error for magnesium, it is difficult to determine conclusively whether this difference alone affects γ . Therefore, the rate of reduction in the growth rate and the rate of change in β were carefully estimated against various combinations of f and δ in the presence of magnesium. The result led to the conclusion that, in the case of magnesium, the difference between the γ values is not significant.

Therefore, while zinc and magnesium reduce the face growth rate by reducing the step velocity of the formed two-dimensional nucleus, it is thought that they do

not affect the edge free energy. This implies that both impurities have almost no effect on the nucleation frequency (at least for the range of concentrations tested). This conclusion is consistent with the morphology of HAP seen in bone tissue. If zinc and magnesium do not affect the nucleation frequency of HAP crystals but rather only suppress the growth of precipitated crystals, likely result is the formation of numerous nano-sized HAP crystals, as seen in human bone. If zinc and magnesium had no evident impurity effect for growth, HAP crystals would easily become enlarged, and the combined strength and flexibility originally possessed by bone might be lost.

In growth rate measurement experiments in the presence of impurities using the phase-shift method, investigations have been carried out on adsorption mechanism using Langmuir and Temkin isotherms as well as on the chemical morphologies of adsorbed zinc and magnesium [71]. A Langmuir-type adsorption model for kinks was determined to be appropriate on the basis of model fitting in which impurities adsorb onto the kink sites in the step front and onto the terraces between steps.

In contrast to detailed growth rate measurements for the *c*-face, there are no reports on the growth rate of the *a*-face. As mentioned previously, the reason for this is the lack of reliable data due the fact that the growth rate of the *a*-face is more than 1 order of magnitude lower than that of the *c*-face. Observations based on AFM have been reported for the growth mode of the *a*-face [77]. Under similar experimental conditions as those for the *c*-face (growth in pseudo body fluid), growth by step movement occurs on the *a*-face. Although it has not been directly proven that this step originates from spiral dislocation, spiral growth probably occurs because the growth proceeds with the filling of etch pits on the surface. The dependence of the step velocity on the supersaturation, as well as changes in velocity associated with changes in the step spacing, has been measured, and the surface diffusion length was concluded to be only a few nanometers.

3.4.7 Discussion of HAP Growth Unit

In discussing crystal growth mechanisms, the growth unit (that which serves as the minimal unit of growth) is generally considered to be an atom or molecule. In this model, growth of soluble inorganic salts is assumed to proceed as a result of positive or negative ions being incorporated into the crystal lattice. However, depending on the type and growth environment of the crystals, there are instances in which the experimental data are better explained by considering the growth unit as a far larger assembly than an atom or molecule [78–80]. Such a cluster is composed of aggregates of atoms or molecules and has a defined structure, unlike random aggregates.

The concept of the cluster itself is very old. For example, even when the term cluster was not in widespread use, there had been attempts to explain the mosaic structure displayed by NaCl crystals growing in aqueous solution with a growth model incorporating units called block nuclei. Biominerals, including HAP, are

examples for which growth models with clusters as units are thought to fit the data well. Viewed qualitatively, a number of reasons for this may be offered. Examples include (1) an extremely low growth rate despite the high supersaturation, (2) difficulty growing giant crystals that retain high crystallinity under normal temperature and pressure, and (3) ease of producing an amorphous phase. These characteristics reflect phenomena observed in the growth of protein crystals. In proteins, in which growth proceeds as a result of the aggregation of giant molecules, two types of growth driving forces need to be considered: supersaturation, which is determined thermodynamically, and intermolecular interactions. The latter factor is normally not considered in the growth of ionic crystals. If we imagine the simplest situation, intermolecular interactions are determined by the competition of repulsive forces due to the average charge of the molecular surface and the van der Waals attraction force between molecules. When intermolecular interactions are involved, complex phenomena arise. For example, even under conditions of very high concentrations of the solute itself, the growth rate becomes extremely low when very weak attractive interaction operates, and sometimes no crystal growth occurs and only an amorphous phase precipitates due to the solubility difference between crystal and amorphous phases. Therefore, if biomineral growth proceeds in a manner similar to that of protein crystal growth, the growth unit should be considered as an aggregate (a cluster) and there is intermolecular interaction between units.

Two lines of circumstantial evidence can be offered for the suggestion that the growth unit for HAP (at least in environments resembling those within the human body) takes the form of a cluster. The first involves the physical constants related to growth. The values for the edge free energy and the step kinetic coefficients diverge widely from typical values for soluble inorganic crystals and, in fact, are closer to those of protein crystals [77]. The second is that dynamic light-scattering measurements of pseudo-body fluid show the existence of aggregates with a hydrodynamic radius of about 0.5 nm [81,82]. Since these aggregates disappear when calcium or phosphate ions are removed from the solution, it is highly likely that they are calcium phosphate clusters. Initially, these clusters were thought to be Posner clusters ($\text{Ca}_9(\text{PO}_4)_6$), and a crystal growth model based on the simple aggregation of clusters was proposed.

When assuming the presence of Posner clusters within the HAP crystal structure, it is possible to define two types of chiral clusters. The two types correspond to the L- and D-forms of amino acids and comprise structures with threefold symmetry in which six phosphate ions are arranged around the calcium ion at the center of the cluster. An ab initio calculation was performed to estimate whether or not a structure with the chemical composition $\text{Ca}_9(\text{PO}_4)_6$ could exist in a stable form. In this calculation, the relative energies of clusters were compared by obtaining stable structures of $\text{Ca}_3(\text{PO}_4)_2$ [83], and then combining up to four of these structures [84–86]. First, energy calculations were performed for $\text{Ca}_3(\text{PO}_4)_2$ (corresponding to the monomer), taking into consideration the spatial arrangements (three types) that could be assumed given a pair of calcium and phosphate ions. Ten types of isomers with a local energy minimum were defined. Among these, an isomer with D_{3h} symmetry and basket-like morphology was overwhelmingly stable compared

to the others, so this isomer was established as the monomer. After two, three, and four of these monomers were combined in simple combinations, the cluster energy decreased monotonically with the number of monomers. However, comparison of the energies for structures with the most compact morphology at each number combination showed that the minimum energy was attained with a $\text{Ca}_9(\text{PO}_4)_6$ trimer. The structure of $\text{Ca}_9(\text{PO}_4)_6$ in this case has a T_h symmetry, and, when refined to take up the minimum energy structure on the potential energy surface (PES), it shows an S_6 symmetry.

Although 24 types of isomers with a local energy minimum appear on the $\text{Ca}_9(\text{PO}_4)_6$ PES, among these, S_6 is a special structure that has nearly the lowest energy despite its extremely high symmetry. From these results, it was determined that if clusters are considered as the growth units for HAP, S_6 is the most appropriate structure. It has sixfold symmetry, and the crystal structure of HAP cannot be constructed by aggregating these clusters. However, simply by slightly rotating the surrounding phosphate ions relative to the calcium ion at the center of the cluster, the cluster can be changed into a Posner cluster with threefold symmetry. Depending on whether the direction of rotation is clockwise or counterclockwise, it is possible to bestow chirality to the cluster as well. The energy required for this rotation is 10 kcal or less and is not a barrier to structural conversion. The above-mentioned calculation results all presume treatment in vacuum, and no conclusions have yet been reached on whether or not the S_6 structure stably exists in actual solutions.

Highly intriguing research results have been reported for the growth units of biominerals, including HAP [87]. In this research, a diluted solution of calcium chloride was gradually added to a diluted carbonate buffer solution under constant pH conditions and changes in the solution concentration of calcium ions were measured using a calcium ion electrode. Even when the solution condition was undersaturated for calcium carbonate salts (such as calcite), the rate of increase in free calcium ions was considerably lower than the value calculated from the amount of calcium ions added (Fig. 3.4a). In other words, many of the added calcium ions were in a bound state and were consumed by the formation of some sort of assembly. A further important point is that the rate of increase in free calcium ions was nearly constant as the solution transitioned from an undersaturated state to a supersaturated state as a result of calcium ion addition until immediately before nucleation occurred. These results indicate that calcium carbonate clusters in solution are already in the undersaturated state and that their aggregation (or an increase in their size) causes nucleation. Although the appearance of metastable clusters during the course of nucleation is also considered in classical nucleation models, unlike these types, the above-mentioned clusters are energetically stable (in local energy-minimum state).

In this research, attempts were made to measure the size of the clusters using analytical ultracentrifugation. This method measures the diffusion coefficients from the precipitation rate of the clusters formed by centrifugation. Like the dynamic light-scattering method, the measured diffusion coefficients are converted into a hydrodynamic radius in accordance with the Stokes–Einstein equation. In an undersaturated solution, clusters were not detected because of the low concentration;

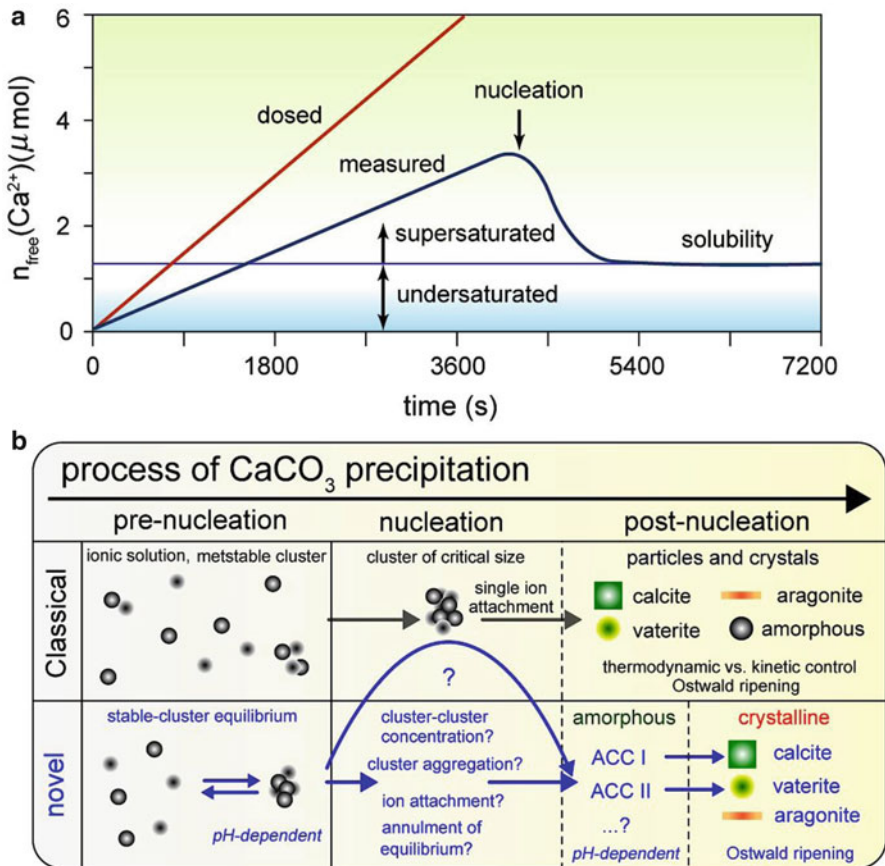


Fig. 3.4 (a) Time-dependent amount of free calcium ions measured in the solution (blue) using calcium ion selective electrode in comparison with dosed amount of calcium ions (red). (b) Schematic image of novel nucleation process through thermodynamically stable calcium carbonate clusters in comparison with classical nucleation process (reproduced with permission from [87]) (copyright 2008, American Association of Advancement of Science)

however, in a supersaturated solution, immediately before nucleation, clusters with a radius of 1 nm were detected. Furthermore, while the incidence was low, the existence of clusters with a radius of about 2 nm was also suggested.

Immediately after nucleation, the clusters further increased in size. There was variation in the structure of the clusters, meaning that it was possible that these different clusters ultimately formed different polymorphs of calcium carbonate—i.e., calcite, vaterite, and aragonite—through the formation of amorphous phases differing in structure (Fig. 3.4b). This idea clearly differs from classical models, which assume that the final crystal polymorph types are determined after nucleation.

In terms of the association between the macroscopic morphology of the produced crystal and the growth unit, Banfield et al. suggested that natural biomineralization

processes proceed in an aggregation-based manner and result in the construction of characteristic fine structures [88]. Gebauer et al., using methods similar to those mentioned above, conducted measurements on calcium phosphate solutions and have confirmed the presence of clusters in this case as well. Given the various lines of experimental evidence presented in recent years, it appears almost certain that clusters are involved in some way in the growth of insoluble biominerals.

3.5 Future Perspectives

The crystal growth of HAP does not qualitatively differ from that of either soluble inorganic crystals or organic crystals. In other words, spiral growth mediated by dislocation having spiral components or growth by two-dimensional nucleation occurs. This is supported by surface observations of growing crystals. Regarding the rate-limiting process of growth, although incorporation of a growth unit into the crystal requires the highest energy, whether or not this incorporation proceeds through surface diffusion is unclear. The diffusion length is probably minimal. The important point is not in the growth mode but that classical growth models—i.e., models in which growth proceeds as a result of ionic bonds—may not be applicable. This is a problem that is not limited to HAP but also applies to biominerals in general. In the aforementioned cases where growth occurred with cluster units, how the driving force of growth is defined is very important. Depending on the definition, the values for the various physical constants involved in growth, which have been reported in studies to date, may change substantially. Furthermore, it is likely that the problem of how to quantify the intermolecular interactions between clusters and then relate them to growth features will become an issue as well. As mentioned above, the crystallization process for proteins is qualitatively the same as for soluble salts but the growth features are complex because intermolecular interactions are included as a growth factor. With intermolecular interactions, the magnitude of the Hamaker constant (a constant indicative of the van der Waals attraction force) of a molecule has a powerful effect. In biomineral growth as well, it will likely be necessary to conduct tests on the Hamaker constant for each cluster in order to understand the growth mechanisms completely and to clarify the relationship between the final product and the growth unit.

References

1. Newman, W.F., Newman, M.W.: The chemical dynamics of bone mineral. University Chicago Press, Chicago (1958)
2. Aoki, H.: *Kyoi no Seitai Busshitsu Apatite* (in Japanese). Ishiyaku Publishers Inc., Tokyo (1999)
3. Elliot, J.C.: Structure and chemistry of the apatites and other calcium orthophosphates. Elsevier, Amsterdam (1994)

4. Wang, L., Nancollas, G.H.: Calcium orthophosphates: crystallization and dissolution. *Chem. Rev.* **108**, 4628–4669 (2008)
5. Combes, C., Rey, C.: Amorphous calcium phosphates: synthesis, properties and uses in biomaterials. *Acta Biomaterialia* **6**(9), 3362–3378 (2010)
6. Elliot, J.C.: Monoclinic space group of hydroxyapatite. *Nature* **230**, 72 (1971)
7. Posner, A.S., Perloff, A., Diorio, A.F.: Refinement of the hydroxyapatite structure. *Acta Cryst.* **11**, 308–309 (1958)
8. Elliot, J.C., Mackie, P.E., Young, R.A.: Monoclinic hydroxyapatite. *Science* **180**, 1055–1057 (1973)
9. Bauer, M.: Röntgenographische und Dielektrische Untersuchungen an Apatiten. Dissertation, Fakultät für Physik, Universität Karlsruhe (1991)
10. Dallemagne, M.J., Richelle, L.J.: Inorganic chemistry of bone. Biological mineralization, pp. 23–42. Wiley, New York (1973)
11. Weatherell, J.A., Robinson, C.: The inorganic composition of teeth. Biological mineralization, pp. 43–74. Wiley, New York (1973)
12. Bienenstock, A., Posner, A.S.: Calculations of the X-ray intensities from arrays of small crystallites of hydroxyapatite. *Arch. Biochem. Biophys.* **124**, 604–607 (1968)
13. Eanes, E.D., Gillissen, I.H., Posner, A.S.: Intermediate states in the precipitation of hydroxyapatite. *Nature* **208**, 365–367 (1965)
14. Termine, J.D., Posner, A.S.: Calcium phosphate formation in vitro. I. Factors affecting initial phase separation. *Arch. Biochem. Biophys.* **140**, 307–317 (1970)
15. Termine, J.D., Eanes, E.D.: Comparative chemistry of amorphous and apatitic calcium phosphate preparations. *Calcif. Tissue. Res.* **10**, 171–197 (1972)
16. Dorozhkin, S.V., Epple, M.: Biological and medical significance of calcium phosphates. *Angew. Chem. Int. Ed.* **41**, 3130–3146 (2002)
17. Christoffersen, J., Christoffersen, M.R., Kibalczyk, W., Andersen, A.: A contribution of understanding of the formation of calcium phosphates. *J. Cryst. Growth* **94**, 767–777 (1989)
18. Christoffersen, J., Christoffersen, M.R., Kibalczyk, W.: Apparent solubilities of two amorphous calcium phosphates and of octacalcium phosphate in the temperature range 30–42°C. *J. Cryst. Growth* **106**, 349–354 (1990)
19. Posner, A.S., Betts, F.: Synthetic amorphous calcium phosphate and its relation to bone mineral. *Accounts Chem. Res.* **8**, 273–281 (1975)
20. Tropp, J., Blumenthal, N.C., Waugh, J.S.: Phosphorous NMR study of solid amorphous calcium phosphate. *J. Am. Chem. Soc.* **105**, 22–26 (1983)
21. Harries, J.E., Hukins, D.W.L., Hasnain, S.S.: Analysis of the EXAFS spectrum of hydroxyapatite. *Mater. Res. Bull.* **9**, 353–360 (1986)
22. Harries, J.E., Hukins, D.W.L., Holt, C., Hasnain, S.S.: Conversion of amorphous calcium phosphate into hydroxyapatite investigated by EXAFS spectroscopy. *J. Cryst. Growth* **84**, 563–570 (1987)
23. Peters, F., Schwarz, K., Epple, M.: The structure of bone studied with synchrotron X-ray diffraction, X-ray absorption spectroscopy and thermal analysis. *Thermochim. Acta.* **361**, 131–138 (2000)
24. Onuma, K., Oyane, A., Tsutsui, K., Tanaka, K., Treboux, G., Kanzaki, N., Ito, A.: Precipitation kinetics of hydroxyapatite revealed by the continuous-angle laser light-scattering technique. *J. Phys. Chem. B* **104**, 10563–10568 (2000)
25. Pan, H.-B., Darvell, B.W.: Calcium phosphate solubility: the need for re-evaluation. *Cryst. Growth & Des.* **9**, 639–645 (2009)
26. Burton, W.K., Cabrera, N., Frank, F.C.: The growth of crystals and the equilibrium structure of their surfaces. *Phil. Trans. Roy. Soc. London* **A234**, 299–358 (1951)
27. Bennema, P.: Crystal growth measurements on potassium aluminium alum and sodium chlorate from slightly supersaturated solutions. *Phy. Stat. Solidi.* **17**, 563–570 (1966)
28. Denk Jr., E.G., Botsaris, G.D.: Mechanisms of potassium alum crystal growth from solution. *J. Cryst. Growth* **6**, 241–244 (1970)

29. Gilmer, G.H., Ghez, R., Cabrera, N.: An analysis of combined surface and volume diffusion processes in crystal growth. *J. Cryst. Growth* **8**, 79–93 (1971)
30. Chernov, A.A.: The spiral growth of crystals. *Sov. Phys. Usp.* **4**, 116–148 (1961)
31. Sunagawa, I., Tsukamoto, K.: Growth spirals on NaCl and KCl crystals growth from solution phase. *J. Cryst. Growth* **15**, 73–78 (1972)
32. Van Enckevort, W.J.P., Bennema, P., van der Linden, W.H.: On the observation of growth spirals with very low step heights on potassium alum single crystals. *Z. Phys. Chem.* **124**, 171–191 (1981)
33. Jetten, L.A.M.J., van der Hoek, B., van Enckevort, W.J.P.: In situ observations of the growth behavior of the {010} face of potassium hydrogen phthalate. *J. Cryst. Growth* **62**, 593–611 (1983)
34. Van Enckevort, W.J.P., Klapper, H.: Observation of growth steps with full and half unit cell heights on the {011} faces of NiSO₄·6H₂O in relation to the defect structure. *J. Cryst. Growth* **80**, 91–103 (1987)
35. Van Erk, W., van Hoek-Martens, H.J.G.J., Bartels, G.: The effect of substrate orientation on the growth kinetics of garnet liquid phase epitaxy. *J. Cryst. Growth* **48**, 621–634 (1980)
36. Chernov, A.A., Rashkovich, L.N., Mkrtchan, A.A.: Solution growth kinetics and mechanism: prismatic face of ADP. *J. Cryst. Growth* **74**, 101–112 (1986)
37. Chernov, A.A., Rashkovich, L.N.: Spiral crystal growth with nonlinear dependence of step growth rate on supersaturation; the {110} faces of KH₂PO₄ crystals in aqueous solution. *J. Cryst. Growth* **84**, 389–393 (1987)
38. Maiwa, K., Tsukamoto, K., Sunagawa, I.: Activities of spiral growth hillocks on the (111) faces of barium nitrate crystals growing in an aqueous solution. *J. Cryst. Growth* **102**, 43–53 (1990)
39. Onuma, K., Tsukamoto, K., Sunagawa, I.: Growth kinetics of K-Alum crystal in relation to the surface supersaturations. *J. Cryst. Growth* **100**, 125–132 (1990)
40. Vekilov, P.G., Kuznetsov, Y.G., Chernov, A.A.: Interstep interaction in solution growth; (101) ADP face. *J. Cryst. Growth* **121**, 643–655 (1992)
41. Malkin, A.I., Chernov, A.A., Alexeev, I.V.: Growth of dipyramidal face of dislocation-free ADP crystals; free energy of steps. *J. Cryst. Growth* **97**, 765–769 (1989)
42. Mullin, J.W.: *Crystallization*, 4th edn, p. 130. Butterworth-Heinemann, Oxford (2001)
43. Robinson, R.: *The significance of phosphate esters in metabolism*. New York University Press, New York (1932)
44. Brighton, C.T., Hunt, R.M.: Mitochondrial calcium and its role in calcification. Histochemical localization of calcium in electron micrographs of the epiphyseal growth plate with K-pyroantimonate. *Clin. Orthop.* **100**, 406–416 (1974)
45. Farley, J.R., Baylink, D.J.: Purification of skeletal growth factor from human bone. *Biochemistry* **21**, 3205–3207 (1982)
46. Moreno, E.C., Zahradnik, R.T., Glazman, A., Hwu, R.: Precipitation of hydroxyapatite from dilute solutions upon seeding. *Calcif. Tissue Res.* **24**, 47–57 (1977)
47. Tomson, M.B., Nancollas, G.H.: Mineralization kinetics: a constant composition approach. *Science* **200**, 1059–1060 (1978)
48. Koutsoukos, P., Amjad, Z., Tomson, M.B., Nancollas, G.H.: Crystallization of calcium phosphate. A constant composition study. *J. Am. Chem. Soc.* **102**, 1553–1557 (1980)
49. Moreno, E.C., Varughese, K.: Crystal growth of calcium apatites from dilute solutions. *J. Cryst. Growth* **53**, 20–30 (1981)
50. Arends, J., Christoffersen, J., Christoffersen, M.R., Eckert, H., Fowler, B.O., Heughebaert, J.C., Nancollas, G.H., Yesinowski, J.P., Zawacki, S.J.: A calcium hydroxyapatite precipitated from an aqueous solution: an international multimethod analysis. *J. Cryst. Growth* **84**, 515–532 (1987)
51. Christoffersen, M.R., Christoffersen, J.: A revised theory for the growth of crystals by surface nucleation. *J. Cryst. Growth* **121**, 608–616 (1992)
52. Christoffersen, M.R., Christoffersen, J.: Possible mechanism for the growth of the biomaterial, hydroxyapatite microcrystals. *J. Cryst. Growth* **121**, 617–630 (1992)

53. Hayek, E., Lechleitner, J., Böhler, W.: Hydrothermalsynthese von Hydroxylapatit. *Angew. Chem.* **67**, 326 (1955)
54. Hayek, E., Böhler, W., Lechleitner, J.: Hydrothermalsynthese von Calcium-Apatiten. *Z. Anorg. Allg. Chem.* **295**, 241–246 (1958)
55. Perloff, A., Posner, A.S.: Preparation of pure hydroxyapatite crystals. *Science* **124**, 583–584 (1956)
56. Simpson, D.R.: Carbonate in hydroxyapatite. *Science* **147**, 501–502 (1965)
57. Jullman, H., Mosebach, R.: Zur Synthese, Licht- und Doppelbrechung des Hydroxylapatits. *Z. Naturf.* **21**, 493–494 (1966)
58. Blakeslee, K.C., Condrate, R.A.: Vibration spectra of hydrothermally prepared hydroxyapatite. *J. Am. Ceram. Soc.* **54**, 559–563 (1971)
59. Baumer, A., Argiolas, R.: Synthèses hydrothermales et déterminations RX d'apatites chlorée, fluoree ou hydroxylée. *Neues Jb. Miner. Mh.* 344–348 (1981)
60. Mengeot, M., Harvill, M.L., Gilliam, O.R.: Hydrothermal growth of calcium hydroxyapatite single crystals. *J. Cryst. Growth* **19**, 199–203 (1973)
61. Arends, J., Schthof, J., van der Linden, W.H., Bennema, P., van den Berg, P.J.: Preparation of pure hydroxyapatite single crystals by hydrothermal recrystallization. *J. Cryst. Growth* **46**, 213–220 (1979)
62. Ito, A., Nakamura, S., Aoki, H., Akao, M., Teraoka, K., Tsutsumi, S., Onuma, K., Tateishi, T.: Hydrothermal growth of carbonate-containing hydroxyapatite single crystals. *J. Cryst. Growth* **163**, 311–317 (1996)
63. Mengeot, M.: Hydrothermal growth and electron-spin-resonance investigations of calcium hydroxyapatite single crystals. PhD Thesis, University of Connecticut (1975)
64. Eysel, W., Roy, D.M.: Hydrothermal flux growth of hydroxyapatites by temperature oscillation. *J. Cryst. Growth* **20**, 245–250 (1973)
65. Nakadate, S., Yamaguchi, I.: Japanese patent laid-open. H02-287107, (1990)
66. MacInnis, I., Onuma, K., Tsukamoto, K.: In situ study of dissolution kinetics of calcite crystal using phase shift interferometry. In: *Proceedings Sixth Topical Meeting on Crystal Growth Mechanism*, pp. 233–238 (1993)
67. Maruyama, M., Tsukamoto, K., Sazaki, G., Nishimura, Y., Vekilov, P.: Chiral and achiral mechanisms of regulation of calcite crystallization. *Cryst. Growth & Des.* **9**, 127–135 (2009)
68. Kanzaki, N., Onuma, K., Ito, A., Teraoka, K., Tateishi, T., Tsutsumi, S.: Direct growth rate measurement of hydroxyapatite single crystal by Moire phase shift interferometry. *J. Phys. Chem. B* **102**, 6471–6476 (1998)
69. Onuma, K., Kanzaki, N., Ito, A., Tateishi, T.: Growth kinetics of hydroxyapatite (0001) face revealed by phase shift interferometry and atomic force microscopy. *J. Phys. Chem. B* **102**, 7833–7838 (1998)
70. Markov, I.V.: *Crystal growth for beginners: fundamental of nucleation, crystal growth and epitaxy*. World Scientific Publishing, Singapore (1995)
71. Kanzaki, N., Onuma, K., Treboux, G., Tsutsumi, S., Ito, A.: Inhibitory effect of magnesium and zinc on crystallization kinetics of hydroxyapatite (0001) face. *J. Phys. Chem. B* **104**, 4189–4194 (2000)
72. Kanzaki, N., Onuma, K., Treboux, G., Tsutsumi, S., Ito, A.: Effect of impurity on two-dimensional nucleation kinetics: case studies of magnesium and zinc on hydroxyapatite (0001) face. *J. Phys. Chem. B* **105**, 1991–1994 (2001)
73. Amjad, Z., Koutsoukos, P., Nancollas, G.H.: The crystallization of hydroxyapatite and fluorapatite in the presence of magnesium ions. *J. Colloid Interface Sci.* **101**, 250–256 (1984)
74. Dalpi, M., Karayianni, E., Koutsoukos, P.: Inhibition of hydroxyapatite formation in aqueous solutions by zinc and 1,2-dihydroxy-1,2-bis(dihydroxyphosphonyl)ethane. *J. Chem. Soc. Faraday Trans.* **89**, 965–969 (1993)
75. Fuierer, T.A., LoRe, M., Puckett, S.A., Nancollas, G.H.: A mineralization adsorption and mobility study of hydroxyapatite surfaces in the presence of zinc and magnesium. *Langmuir* **10**, 4721–4725 (1994)

76. Liu, X.Y., Maiwa, K., Tsukamoto, K.: Heterogeneous two-dimensional nucleation and growth kinetics. *J. Chem. Phys.* **106**, 1870–1879 (1997)
77. Onuma, K., Ito, A., Tateishi, T., Kameyama, T.: Growth kinetics of hydroxyapatite revealed by atomic force microscopy. *J. Cryst. Growth* **154**, 118–125 (1995)
78. Horn, D., Rieger, J.: Organic nanoparticles in the aqueous phase—theory, experiment, and use. *Angew. Chem. Int. ed.* **40**, 4330–4361 (2001)
79. Furrer, G., Phillips, B.L., Ulrich, K.U., Pothig, R., Casey, W.H.: The origin of aluminum flocs in polluted streams. *Science* **297**, 2245–2247 (2002)
80. Navrotsky, A.: Energetic clues to pathways to biomineralization: precursors, clusters, and nanoparticles. *Proc. Natl. Acad. Sci. U. S. A.* **101**, 12096–12101 (2004)
81. Onuma, K., Ito, A.: Cluster growth model for hydroxyapatite. *Chem. Mat.* **10**, 3346–3351 (1998)
82. Oyane, A., Onuma, K., Kokubo, T., Ito, A.: Clustering of calcium phosphate in the system $\text{CaCl}_2\text{-H}_3\text{PO}_4\text{-KCl-H}_2\text{O}$. *J. Phys. Chem. B* **103**, 8230–8235 (1999)
83. Treboux, G., Kanzaki, N., Onuma, K., Ito, A.: Energy-preminent isomer of the $\text{Ca}_3(\text{PO}_4)_2$ cluster. *J. Phys. Chem. A* **103**, 8118–8120 (1999)
84. Treboux, G., Layrolle, P., Kanzaki, N., Onuma, K., Ito, A.: Existence of Posner's cluster in vacuum. *J. Phys. Chem. A* **104**, 5111–5114 (2000)
85. Treboux, G., Layrolle, P., Kanzaki, N., Onuma, K., Ito, A.: Symmetry of Posner's cluster. *J. Am. Chem. Soc.* **122**, 8323–8324 (2000)
86. Kanzaki, N., Treboux, G., Onuma, K., Tsutsumi, S., Ito, A.: Calcium phosphate clusters. *Biomaterials* **22**, 2921–2929 (2001)
87. Gebauer, D., Völkel, A., Cölfen, H.: Stable prenucleation calcium carbonate clusters. *Science* **322**, 1819–1822 (2008)
88. Banfield, J.F., Welch, S.A., Zhang, H., Ebert, T.T., Penn, R.L.: Aggregation-based crystal growth and microstructure development in natural iron oxyhydroxide biomineralization products. *Science* **289**, 751–754 (2000)